Properties and Parameterization of the Stable Boundary Layer over Moderate Topography

A. R. BROWN AND N. WOOD

Met Office, Bracknell, Berkshire, United Kingdom

(Manuscript received 30 January 2003, in final form 14 May 2003)

ABSTRACT

Numerical simulations are used to investigate the impact on the stable boundary layer of moderate topography (with hill heights in some cases comparable to the undisturbed boundary layer depth). Area-averaged properties of the resulting boundary layers, which are often highly inhomogeneous, are diagnosed. The presence of the hills leads to enhanced turbulence and drag, and a deepening of the area-averaged boundary layers (over and above that due to a simple displacement effect). The ability of well-established formulas for the depth of the boundary layer over homogeneous terrain to predict this deepening is investigated. Finally, the implications of the results for the use in large-scale weather and climate prediction models of effective roughness length parameterizations of the effects of hills are discussed. While not capturing some of the more detailed effects, the simplest approach of using a roughness length independent of stability is found to perform reasonably well in predicting the total surface drag.

1. Introduction

Large-scale weather and climate models often use an enhanced or effective roughness length to simulate the increased surface drag caused by turbulent form drag on unresolved hills in the atmospheric boundary layer (e.g., Milton and Wilson 1996). For neutral conditions this approach has been justified by observational (e.g., Grant and Mason 1990) and numerical (e.g., Wood and Mason 1993) studies, both of which have indicated that the area-averaged boundary layer structure over hills, when suitably scaled, is largely indistinguishable from that over a homogeneous surface. However, although the approach is also applied in stable conditions, observational, numerical, or theoretical support is relatively lacking.

Hunt et al. (1988) extended earlier linear analysis of neutral flow over low-sloped hills to stably stratified flow. Their results indicated that the effects of stratification on the flow structure can be considered to be twofold: a kinematic effect due to the change in the undisturbed profiles and a dynamic effect due to buoyancy forces. The former effect leads to the fractional speedup at the crest of a hill being larger in moderately stable than in neutral conditions, which is consistent with the observations of Frank et al. (1993) and Coppin et al. (1994). Belcher and Wood (1996) extended the linear analysis to obtain a prediction of the variation of the turbulent form drag with stability. Numerical modeling has also been used to complement these theoretical studies of the effects of low hills (e.g., Inglis et al. 1995; Belcher and Wood 1996; Weng et al. 1997).

While the preceding studies have provided many valuable insights, they have been limited to low slopes. For boundary-layer-scale hills with more significant slopes (which are likely to be most important in terms of drag), nonlinear effects will become important. The number of relevant studies in this regime is limited, although Mason (1987) and Holden et al. (2000) have presented measurements of flow and turbulence structure measured in stable conditions in different valleys in South Wales (Sirhowy and Llanthony, respectively), each of which has a horizontal scale of around 2 km and valley floor to hilltop height difference of 200–300 m. Both studies include measurements of stress profiles above the valley, although with shallow and highly horizontally inhomogeneous stable boundary layers over orography, it is not clear that these directly provide any useful information on the area-averaged stress and drag. Other recent studies (e.g., Vosper et al. 2002) have demonstrated that it is possible to measure the pressure drag directly using an array of microbarographs, although these have focused on a rather longer-scale hill where gravity waves play a significant role. The potentially very large parameter space, problems with making representative turbulence measurements in stable conditions (e.g., Derbyshire 1995), and sensitivity of the stable boundary layer in general (Derbyshire and Wood 1994) can also make it hard to draw general conclusions from measurements from a single site or experiment.

Corresponding author address: Dr. A. R. Brown, Met Office, London Road, Bracknell, Berkshire RG12 2SZ, United Kingdom.
E-mail: andy.brown@metoffice.com

Even if we were armed with a perfect parameterization of the pressure force on the surface, there are questions about how this should be implemented in a large-scale model. In particular, it is not clear whether an effective roughness length parameterization (which seeks to represent the effects of hills solely through a change in surface characteristics) can possibly be successful if, in reality, the unresolved hills occupy a significant fraction of the depth of the undisturbed stable boundary layer.

In view of these uncertainties, the present study examines, through a series of deliberately very idealized numerical simulations, the effects of hills (of too short a wavelength to produce gravity waves) on the stable boundary layer. Particular attention is given to the area-averaged properties of the boundary layer, including the surface forces. The ability of the commonly used, effective roughness length parameterization to represent the effects of the hills is investigated. The model and simulations performed are described in section 2. Section 3 contains the results, and conclusions are given in section 4.

2. Model and simulations performed

The simulations presented in this study were performed using the nonlinear BLASIUS model of Wood and Mason (1993), extended to include stability effects as described in Belcher and Wood (1996). It incorporates a one-and-a-half-order turbulence closure, that is, fluxes related to mean gradients through viscosity, but the viscosity itself depends on the turbulent kinetic energy, for which a prognostic equation is carried. The model uses a nonorthogonal coordinate transformation (Clark 1977) such that the model levels are terrain following close to the surface but become horizontal at the top of the domain. In the transformed coordinate system, a staggered orthogonal grid is imposed. The continuous equations are discretized onto this grid using standard finite-difference techniques: the advection terms are centered in time, while a forward time step is used for the diffusion terms; the second-order scheme of Piacsek and Williams (1970) is used for advection of the velocity components, while the monotone ''ULTIMATE-QUICKEST'' scheme of Leonard et al. (1993) is used for advection of the scalar fields. Periodic horizontal boundary conditions are used. The lower boundary condition is no slip, which is applied by assuming Monin–Obukhov similarity between the surface and each of the lowest internal grid points. The upper boundary is formed by a stress-free rigid lid. A sponge layer may be applied in the upper part of the domain, but was not required in the present study because the terrain-induced perturbations did not reach the domain top for the profiles chosen.

Note that density has no dynamic role in the Boussinesq simulations considered and it is set equal to unity. Accordingly, all dynamic quantities considered (e.g., force, stress, pressure) should be interpreted as being per unit density. A Cartesian ($x_1 = x$, $x_2 = y$, $x_3 = z$) coordinate system is used throughout, with the z direction vertical, and the velocity vector has components ($u_1 = u$, $u_2 = v$, $u_3 = w$). The vertical momentum fluxes are τ_{13} and τ_{23}, and h_3 is the vertical buoyancy flux. When diagnosed from the hilly simulations these include the small resolved fluxes (e.g., $u'w'$ where primes indicate perturbations from the horizontal mean) in addition to the turbulent fluxes. Angled brackets (e.g.,$\langle u \rangle$) indicate averages along horizontal surfaces. Finally we define $U_{\rm av}$, $S_{\rm av}$, and $\tau_{\rm av}$, to be equal to the magnitudes of the area-averaged velocity, shear, and stress vectors; that is, $U_{\rm av}^2 = \langle u \rangle^2 + \langle v \rangle^2$, $S_{\rm av}^2 = (\partial\langle u \rangle/\partial z)^2 + (\partial\langle v \rangle/\partial z)^2$ and $\tau_{\rm av}^2 = \langle \tau_{13} \rangle^2 + \langle \tau_{23} \rangle^2$.

One-dimensional simulations were performed first, in order to provide initial conditions for the hilly runs and also to provide results consistent with those of the hilly runs in the limit of the hill height going to zero. The hilly simulations were then run for 18 000 s.

a. One-dimensional simulations

All of the simulations were driven by a large-scale vector pressure gradient, equivalent, at 45°N with a Coriolis parameter of $f = 10^{-4}$ s^{-1}, to a geostrophic wind of magnitude $G = 10$ m s^{-1} aligned with the x axis. The surface roughness length was set to a vegetative value of $z_0 = 0.1$ m. Starting with initial wind components equal to their geostrophic values, and a constant buoyancy profile, the model was run forward in time with an imposed surface buoyancy flux (h_3_surf). This varied between 0.0 m^2 s^{-3} (simulation B0_H0) and -0.0010 m^2 s^{-3} (simulation B10_H0). Note that the simulation naming convention has been chosen so that the buoyancy flux can be immediately ascertained, with Bx indicating that is has a value of $x \times 10^{-4}$ m^2 s^{-3}. Similarly, Hh indicates a hill of crest-to-trough height h m (zero for these one-dimensional runs).

Derbyshire (1990) predicted theoretically that the most negative sustainable turbulent buoyancy flux should be $-(R_{fc}/3^{1/2})G^2|f|$, which, with the value used here of 0.33 for the critical flux Richardson number R_{fc}, gives a value -0.0019 m^2 s^{-3}. However, A. Grant (2002, personal communication) has used the dataset described in Grant (1994) to create a scatterplot of measured nighttime surface buoyancy fluxes at Cardington against 220-m wind speed (used as a surrogate for the geostrophic wind). This showed that, while the bulk of the data did show an approximately quadratic dependence of buoyancy flux on wind speed, the magnitudes of the fluxes were only rarely more than one-quarter of the maximum value predicted by Derbyshire (1990). Accordingly, the range of fluxes covered by simulations B0_H0 to B5_H0 probably covers the most important part of the parameter space for our choice of G and f.

A nonuniform vertical grid was used. This had the lowest grid point at 1 m, with the grid spacing increasing

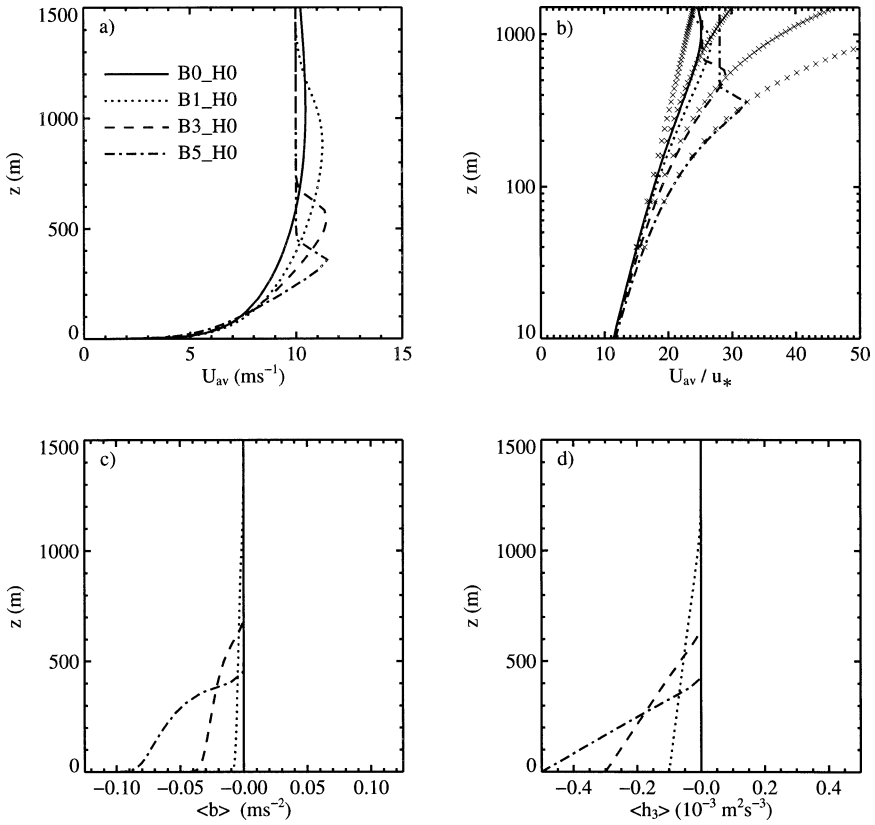

FIG. 1. Profiles from the one-dimensional simulations after 48 000 s (218 000 s for B0_H0): (a) wind speed, (b) normalized wind speed on a logarithmic plot, (c) buoyancy, and (d) buoyancy flux. The crosses in (b) indicate the predictions of Monin–Obukhov theory for the four stabilities used.

to reach 45 m at 300 m above the surface, above which height it was constant up to the domain top at 3000 m. Following Belcher and Wood (1996), the upper limit to the mixing length in the flow interior was set to 100 m, and the critical Richardson number to 0.33.

Profiles from these runs after 30 000 s (200 000 s for B0_H0) were used to initialize the two-dimensional hilly runs. However, all results presented from these runs, were obtained after continuing for a further 18 000 s. This has been done so that the profiles are consistent with those that are obtained after 18 000 s of the hilly runs in the limit of hill height going to zero. Figure 1a shows the wind speed profiles from four of the simulations, and some relevant parameters (friction velocity u_*, Obukhov length L, and boundary layer depth z_i) are given in Table 1. The boundary layer depth (diagnosed as the height at which the total turbulent stress is equal to 5% of its surface value) in the neutral simulation B0_H0 is around 1500 m, but it decreases as expected with increasing surface cooling, and is only 360 m in B5_H0.

TABLE 1. Friction velocity, Obukhov length, boundary layer depth, and scaled boundary layer depth from the one-dimensional runs from which results are presented in Fig. 1.

Run	u_* (m s^{-1})	L (m)	z_i (m)	$z_i/(u_*L/\|f\|)^{1/2}$
B0_H0	0.41	∞	1510	0.00
B1_H0	0.41	1870	960	0.34
B3_H0	0.39	510	550	0.39
B5_H0	0.36	230	360	0.40

Figure 1b shows the same wind profiles, but this time on a logarithmic plot and normalized by u_*. The increase in nondimensional shear with increasing stability can be seen. Furthermore, the results are in good agreement with the predictions of Monin–Obukhov similarity theory in the lower boundary layer for B0_H0 and B1_H0, and throughout most of the boundary layer depth in B3_H0 and B5_H0. The buoyancy profiles (Fig. 1c) show increasing stability within the boundary layer as the surface cooling increases (Fig. 1d) and also a tendency to form a more stable layer at the boundary layer top. Higher up, all retain the neutral static stability initial profiles. This is consistent with Belcher and Wood (1996), although extra sensitivity tests have suggested that the results of the hilly simulations are not particularly sensitive to this choice, with similar results being obtained with constant (nonzero) static stability aloft.

Results will also be shown from some additional one-

dimensional runs performed in order to assess the ability of an effective roughness length parameterization to represent the effects of hills on the area-averaged flow. These were set up in exactly the same way as the standard one-dimensional runs, except with an enhanced or effective roughness length (z_0^{eff}) used instead of the vegetative value of $z_0 = 0.1$ m.

b. Hilly simulations

These simulations were set up in the same way as the one-dimensional simulations from which they took their initial profiles, except that, in the main series of runs, they used 20 evenly spaced grid points in the horizontal to model flow over a single sinusoidal ridge of wavelength $\lambda = 2000$ m and peak-to-trough height h. Due to the periodic boundary conditions, this setup effectively models flow over an infinite series of packed ridges. Note also that the mean height of the surface is zero. Wood and Mason (1993) argued for the effective displacement height in hilly terrain being equal to the mean height of the topography. Hence, assuming that this remains the case in stable conditions, the fact that the mean height is zero means that horizontally averaged statistics at height z can be directly compared with those obtained at the same height above a flat surface.

A large number of simulations were performed, varying h (between 0 and 300 m) for different values of imposed surface buoyancy flux. All were run for 18 000 s and the results shown are from the ends of the simulations. Various extra sensitivity tests were also carried out (e.g., varying λ, and also using more isolated hills) and these will be described in the text when required.

No explicit horizontal diffusion was applied beyond that given by the subgrid model. In a few of the simulations with the smallest hills this meant that the fields became rather noisy close to the boundary layer top. However, these problems disappeared in the simulations with larger hills (which are the main focus of this study) and, in any event, reruns of a couple of simulations with extra diffusion to remove the noise gave very similar results in terms of the drag.

3. Results

a. Flow features

The main focus of the results section will be on area-averaged properties of the boundary layer. However, it is useful to present first some more detailed aspects of the modeled flows, both to give an overview of the cases considered and also to allow comparison with the results of earlier studies.

For the low hills cases, a convenient measure of the effects of the hills is provided by the fractional speedup, defined through

$$\Delta s(x, z') = \frac{u(x, z') - \overline{u(z')}}{\overline{u(z')}}, \qquad (1)$$

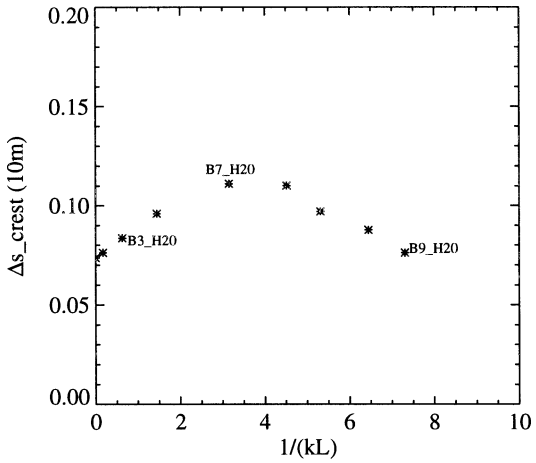

FIG. 2. Fractional speedup at 10 m above the crest as a function of $1/(kL)$ from the simulations of stable flow over a ridge with $\lambda = 2000$ m and $h = 20$ m.

where $\overline{u(z')}$ is the average value of velocity at a fixed height above the local surface (z'). Figure 2 shows the variation of the fractional speedup 10 m above the crest with stability [as measured by $1/(kL)$, where $k = 2\pi/\lambda$ and L is the Obukhov length] for the simulations with $h = 20$ m. It can be seen to increase at first with increasing stability, reaching a maximum at around B7_H20. Although probably a coincidence, it is interesting to note that this change in fractional speedup with stability is resulting almost entirely from changes in the normalizing velocity with stability, with the velocity perturbations themselves being almost independent of stability. However, further increases in stability lead to decreasing velocity perturbations and the fractional speedup decreases once again. This behavior finds some support in the experimental studies of Frank et al. (1993) and Coppin et al. (1994), both of which found fractional speedup increasing at first as stability increased, and then tending to level off (although there was no clear evidence for a decrease) at higher stabilities. Furthermore, although Belcher and Wood (1996) concentrated on pressure drag, the variation in speedup found here is consistent with their arguments: an increase above the neutral value for moderate stabilities due to an increase in the mean shear, followed by a decrease when stability effects are large enough to have a dynamical effect on the perturbations in the outer region.

Note that $1/(kL)$ was used as the nondimensional stability measure for consistency with Belcher and Wood (1996). They found that their results for the pressure drag from sets of runs with varying wavelength approximately collapsed onto one another when plotted in this way. However, this does not appear to be a robust result, as it was not found to be the case for the results for either flow speedup or drag (not shown) from extra runs performed with different wavelength ridges for the present study. Nevertheless, it should be noted that this collapse was never crucial to their arguments. In fact,

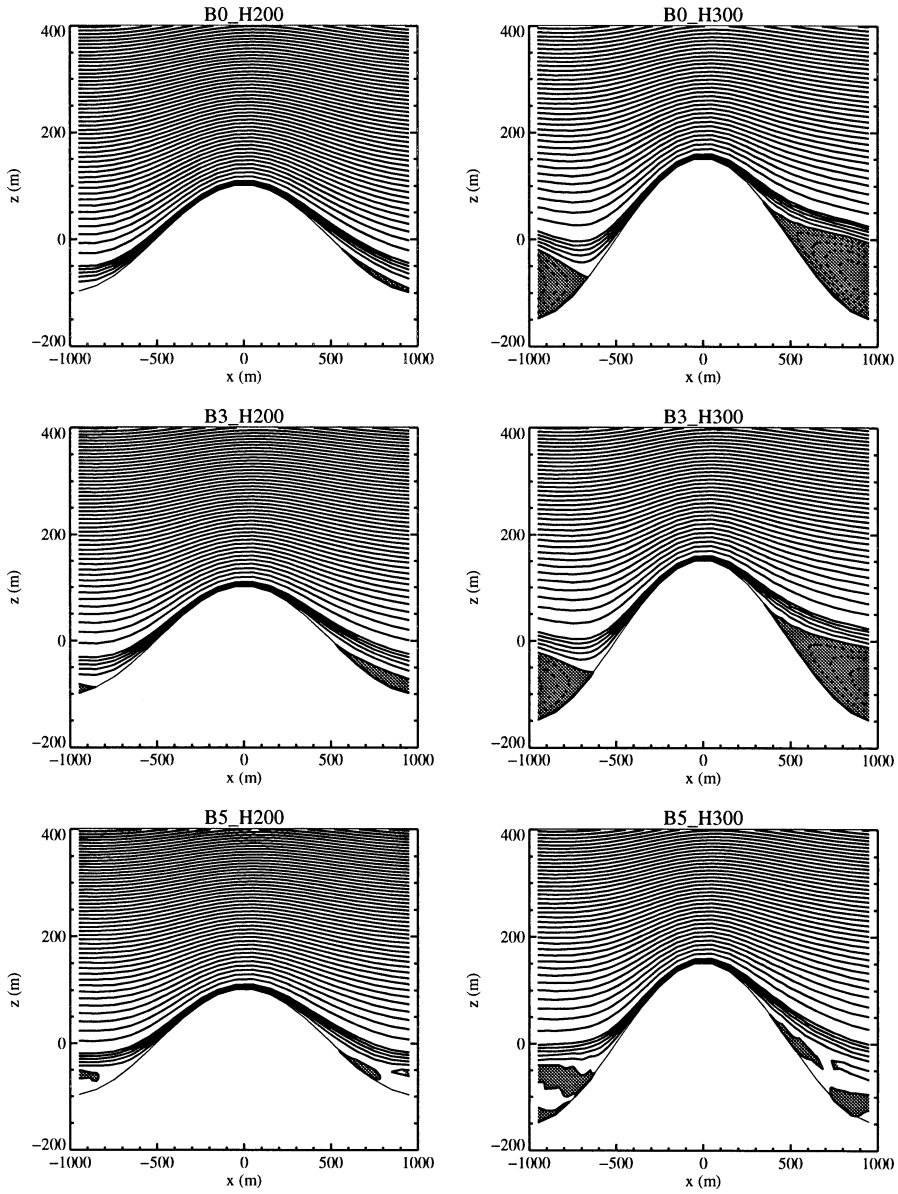

FIG. 3. Streamfunctions from simulations B0_H200, B0_H300, B3_H200, B3_H300, B5_H200, and B5_H300 after 18 000 s. The contour interval is 10 $m^2\ s^{-1}$ for values between 0 and $\pm 50\ m^2\ s^{-1}$, and 50 $m^2\ s^{-1}$ thereafter. Regions with a negative streamfunction are shaded.

the present results are broadly consistent with their suggestion that the maximum value of speedup and pressure drag should occur when the middle layer height (which is the height above which the flow perturbations are asymptotically both inviscid and irrotational) reaches the boundary layer top [as additional increases in $1/(kL)$ cannot further enhance the shear effect]. These sets of runs suggest that the maximum occurs at $1/(kz_i) \simeq 0.8$.

With higher ridges, nonlinear effects start to become increasingly important. Figure 3 shows contours of the streamfunction from the simulations with $h = 200$ and 300 m, for each of three different surface buoyancy fluxes (0.0, -0.0003, and $-0.0005\ m^2\ s^{-3}$). In all cases the contour interval is 10 $m^2\ s^{-1}$ for values between 0 and $\pm 50\ m^2\ s^{-1}$, and 50 $m^2\ s^{-1}$ thereafter. Regions with a negative streamfunction are shaded.

Looking first at the results obtained with $h = 200$ m, note that the neutral simulation (B0_H200) shows just a very small separated region. That this simulation (maximum slope 0.31) should be close to the onset of separation is consistent with the prediction of Wood (1995) that the critical slope for a hill of this wavelength and roughness should be 0.32. The streamline patterns from simulation B3_H200 are quite similar, remaining steady but showing a slightly deeper separated region. Note that a tendency to separate slightly more readily

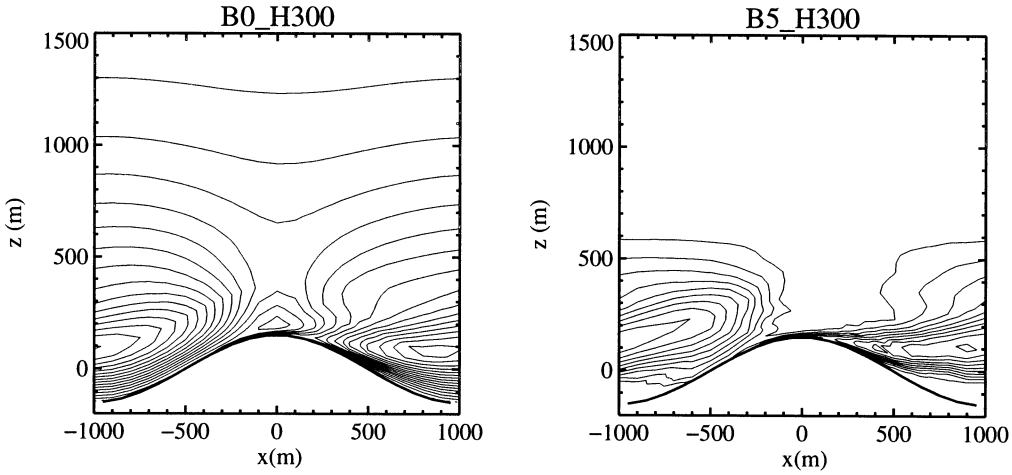

FIG. 4. Contours of τ_{13} from neutral simulation B0_H300 and stable simulation B5_H300. The contour interval is 0.04 $m^2 s^{-2}$.

in stable conditions is what is expected due to the increase in shear in the undisturbed profile. However, the observations from the Sirhowy experiment (Mason 1987) suggested that in that case the effect of stability was to reduce the tendency of the flow to separate. Mason suggested that a possible explanation is that the Sirhowy case had profiles that were stable enough, given the topography of that region, to produce gravity waves and that these destroyed the coherent recirculating region.

With stronger surface cooling (B5_H200), the picture is rather different. For approximately the first hour of this run there was again a coherent separated region (and, due to the increased shear in the undisturbed profile, it was again slightly deeper than before). However, drainage currents then developed and pooling of cold air in the valley led to the formation of a near-stagnant region in the valley (see Fig. 3). This should be contrasted with the coherent recirculation of the less stable simulations.

A similar transition to drainage currents and pooling is seen in the series of simulations with $h = 300$ m. Here the neutral simulation B0_H300 shows a deep separated region, with relatively strong recirculation within the bubble, and B3_H300 shows a similar picture. However, the streamfunction from B5_H300 only appeared similar for approximately the first 1800 s of the simulation, with pooling of cold air then quickly completely removing the coherent recirculation (see Fig. 3). A more detailed analysis of the development of the drainage currents in a single simulation very similar to this run was provided by Wood (1998).

The transition to a regime with essentially decoupled flow above a very stable, almost stagnant region in the valley is broadly consistent with observations from the Llanthony and Sirhowy experiments. For example, Holden et al. (2000) presented stress profiles measured in the Llanthony valley on weakly and strongly stratified nights. In the former case the magnitude of the stress increased gradually with height to reach a maximum at approximately half the hill height above the valley floor before decreasing again. In contrast, the latter case gave very small stresses in the decoupled lowest third of the valley, with the region of significant stress being confined to a relatively narrow region centered at about two-thirds of the hill height. The simulations with $h = 300$ m have a similar geometry to the Llanthony valley, and it is therefore encouraging that a qualitatively similar contrast is visible between the stress contour plots (Fig. 4) from the neutral run B0_H300 and the stable run B5_H300.

The above certainly does not constitute a detailed or quantitative validation of the model, and, particularly for the more stable cases, it will be desirable in the future to perform three-dimensional simulations to allow down-valley flow of the converging drainage currents. The details of the results will also be sensitive to the turbulence closure (Belcher and Wood 1996) and further studies using different closure models or building on recent work using large-eddy simulation (e.g., Henn and Sykes 1999; Calhoun et al. 2001) will be very valuable. Nevertheless, the qualitative agreement of the present simulation results with the observations is encouraging, and suggests that they are sufficiently reliable at least for a first evaluation of the effective roughness length parameterization of the effects of moderate topography in stable conditions.

b. Surface forces

Figure 5 shows the variation with h and h_3_surf of the average surface turbulent shear stresses (τ_{13}_surf, τ_{23}_surf), the average surface pressure force per unit area (F_p), and the normalized pressure force [$\alpha = F_p/(u_{*0}^2\theta^2)$, where u_{*0} is the friction velocity over flat terrain and $\theta(=\pi h/\lambda)$ is the maximum slope of the ridge].

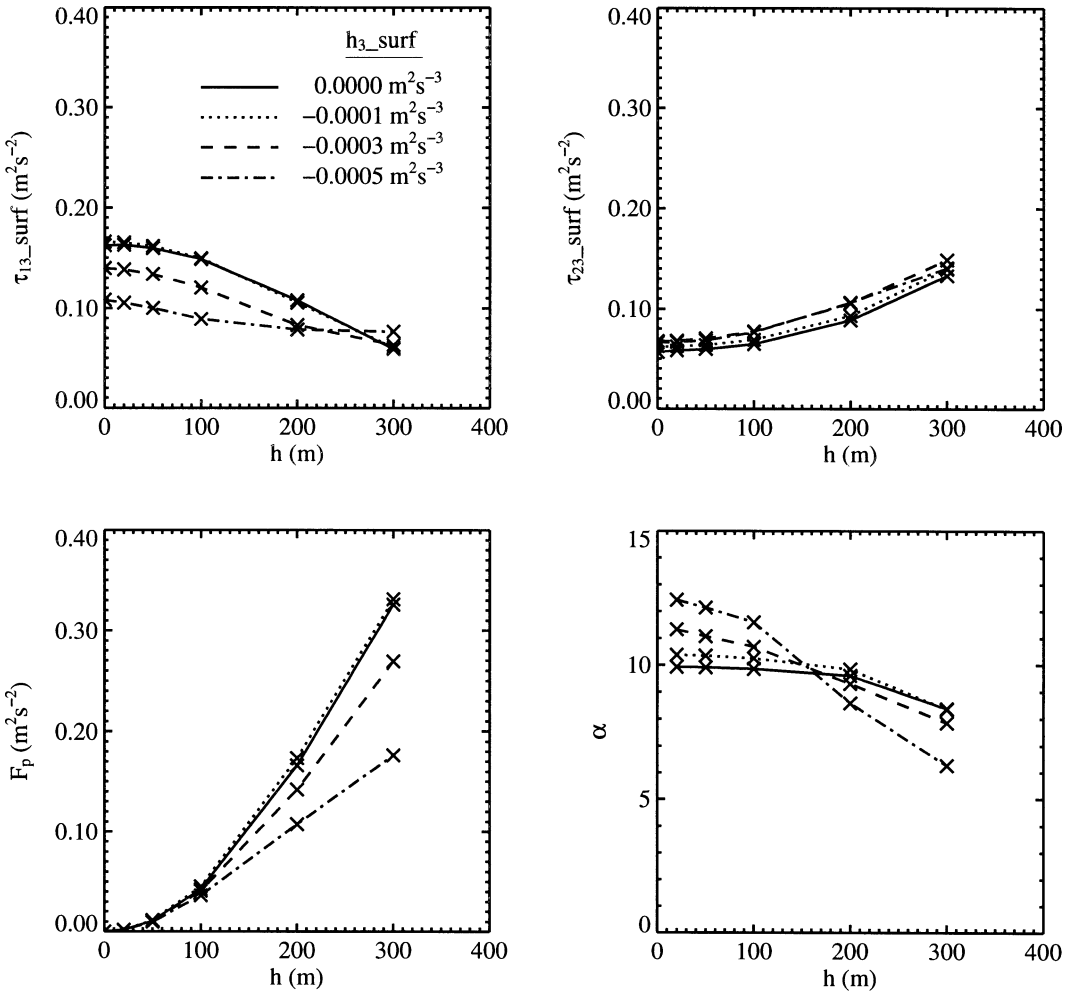

FIG. 5. Average surface turbulent stresses (τ_{13}_surf, τ_{23}_surf), surface pressure force per unit area (F_p), and normalized pressure force (α) as functions of h and h_3_surf.

Wood and Mason (1993) showed that for neutral cases, the change in the total surface drag as h increases is dominated by the increase in F_p; that is, the changes in the surface turbulent stresses are relatively small. Figure 5 confirms that the same is true in stable conditions. For low hills ($h \lesssim 100$ m), F_p is found to be only weakly dependent on stability for the cases shown. However, the decrease in u_{*0}^2 with increasing surface cooling, means that the nondimensional pressure force α increases. More stable cases (not shown) lead to α decreasing again as dynamic buoyancy effects become increasingly important. These results are consistent with those of Belcher and Wood (1996).

For the cases with bigger hills, a stronger dependence of F_p on stability is apparent. For example, B0_H300 has $F_p = 0.33$ m^2 s^{-2} while B5_H300 gives $F_p = 0.18$ m^2 s^{-2}. Although the stability is clearly reducing the value of F_p in simulation B5_H300, it is worth emphasising that its magnitude remains significant (being larger than that of the surface stress over flat terrain). The 45% decrease in F_p in B5_H300 relative to B0_H300 is reflected in a decrease in α, although for these moderate hills, it is not clear that a scaling based on the undisturbed surface stress is most appropriate. Instead, following Wood and Mason (1993) we can write $F_p = 0.5C_d\langle u\rangle^2$ where $\langle u\rangle$ is the area-averaged velocity component at a height of order the hill height, and C_d is a drag coefficient. Within 50 m of the height of the ridge crests, the values of $\langle u\rangle$ from simulations B0_H300 and B5_H300 are within 5% of one another (at around 5 m s^{-1}), and thus the fractional differences in the values of C_d diagnosed from these simulations are similar to those in F_p.

Two extra sensitivity runs were performed based on B0_H300 and B5_H500, but with the hills more isolated. In each case this was done by extending the domain length (and the number of grid points) by a factor of 4, so that a flat plain of length 6000 m separated the base of each hill from that of its periodic image. In this case the effects of the drainage currents in the stable run

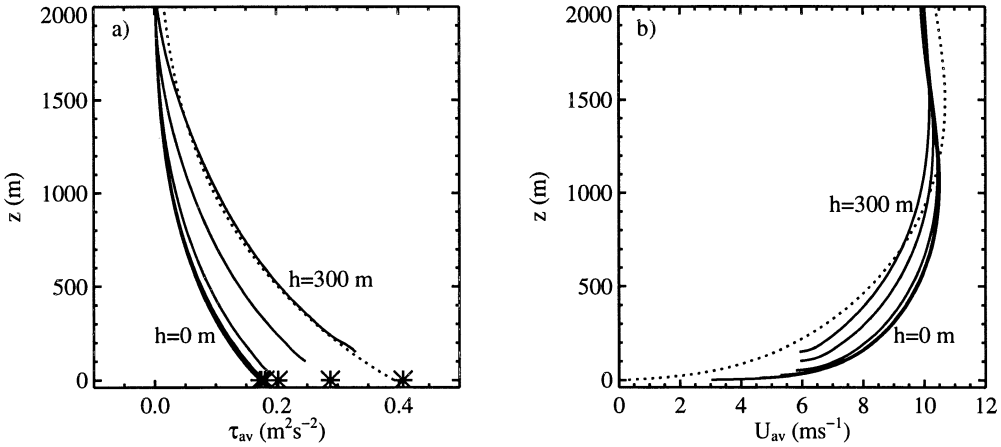

FIG. 6. Results from the neutral simulations with $\lambda = 2000$ m and $h = 0$, 20, 50, 100, 200, and 300 m (solid lines, although note that the 0-, 20-, and 50-m results are almost indistinguishable from one another). Also shown are the results from a neutral one-dimensional simulation with $z_0^{\text{eff}} = 10$ m (dotted lines). (a) The magnitude of the horizontally averaged stress. The asterisks show the total force on the surface (due to shear stress and pressure force) from the hilly simulations. (b) The magnitude of the horizontally averaged wind vector.

were much less marked, with no valley at the foot of the hill in which the cold air could pool. Indeed, a weakly recirculating separated region (much more akin to that in the neutral runs) was maintained on the lee slope. Furthermore, the pressure drag in this stable run was only around 25% smaller than that in the corresponding neutral run. This appears to confirm that the relatively large reduction in F_p in B5_H300 relative to that in B0_H300 is associated with the nonlinear stability effects that lead to the formation of a cold, almost stagnant region in the valley of the former. Note also that it is likely that these two-dimensional simulations exaggerate this effect, as they do not allow outflow of cold air down the main valley.

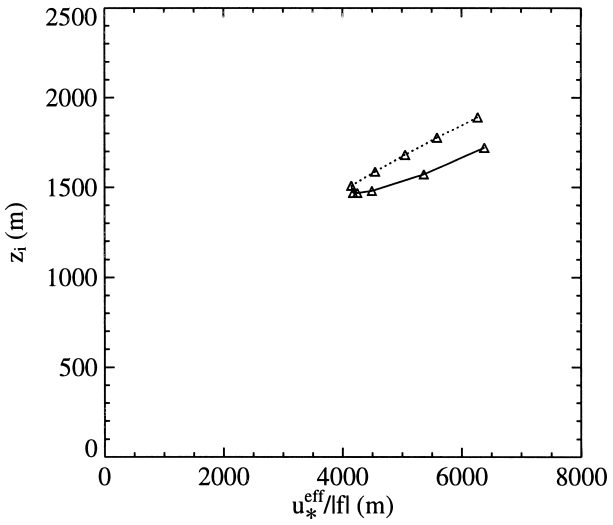

FIG. 7. Boundary layer depth diagnosed from neutral runs as a function of $u_*^{\text{eff}}/|f|$. Solid line indicates results from hilly simulations with varying hill height; dotted line shows results from one-dimensional simulations with effective roughness length varying between 0.1 and 10 m.

c. The area-averaged boundary layer

As noted in the introduction, observational (e.g., Grant and Mason 1990) and numerical (e.g., Wood and Mason 1993) studies have both indicated that the area-averaged neutral boundary layer structure above the hilltops, when suitably scaled, is largely indistinguishable from that over a homogeneous surface. This has been the motivation for the use of effective roughness lengths to parameterize the effects of unresolved hills in large-scale models. The aim of this section is to examine the properties of the area-averaged stable boundary layer, and to assess whether an effective roughness length approach to parameterization remains applicable.

Before examining results from the stable simulations, it is useful as a reference to present first the results obtained in neutral conditions. The flat neutral simulation B0_H0 has a boundary layer depth of 1510 m, and hence even the largest of the simulated hills is comfortably embedded within the boundary layer (e.g., see B0_H300 results in Fig. 4). Figure 6 shows the area-averaged stress and velocity profiles from the neutral runs with varying hill height. Increasing h increases the values of τ_{av} and causes a slight reduction in U_{av} in the boundary layer interior. In all cases the τ_{av} profiles extrapolate down to $(u_*^{\text{eff}})^2$, the magnitude of total force on the surface due to shear stress and pressure force $\{=[(\tau_{13}\text{-surf} + F_p)^2 + \tau_{23}\text{-surf}^2]^{1/2}\}$, at $z = 0$ m. One effect of increasing u_*^{eff} is to cause a slight increase in boundary layer depth. This is visible in Fig. 6a, but is shown more clearly in Fig. 7, which shows z_i [diagnosed as the height at which τ_{av} is equal to $0.05(u_*^{\text{eff}})^2$] as a function of $u_*^{\text{eff}}/|f|$. As the hill height is increased from

0 m ($u_*^{\text{eff}}/|f| = 4100$ m) to 300 m ($u_*^{\text{eff}}/|f| = 6400$ m), z_i increases from 1510 to 1720 m. Such a deepening of the boundary layer due to the pressure force on hills finds support in the experimental results of Hignett and Hopwood (1994), which showed deeper neutral boundary layers for cases with flow normal to ridges than for cases with flow parallel. Note, however, that the simulated hilly boundary layers do not deepen as quickly as predicted by the scale $u_*^{\text{eff}}/|f|$, with an approximately 50% increase in the scale leading to only a 15% increase in z_i.

The effective roughness length parameterization is, as expected, found to work reasonably well for these cases. The dotted lines in Fig. 6 show the results obtained from a one-dimensional simulation with $z_0^{\text{eff}} = 10$ m. This value was chosen as it gives a good match to the value of $(u_*^{\text{eff}})^2$ from simulation B0_H300. The τ_{av} profiles from the hilly and one-dimensional simulations are in excellent agreement, and the U_{av} profiles also match reasonably well [although the agreement is slightly less good than is typically seen for lower-sloped cases, e.g., Wood and Mason (1993)]. Consistent with the good match of the τ_{av} profiles shown in Fig. 6, Fig. 7 shows that the boundary layer depths from the hilly and one-dimensional simulations are similar, with the one-dimensional boundary layers deepening just slightly faster with increasing $u_*^{\text{eff}}/|f|$.

We now consider the results of some of the stable runs. Flat simulation B5_H0 has a boundary layer depth of 360 m, and hence the introduction of a 300-m-high hill is likely to have a significant impact on much of the boundary layer. Figure 4b confirms that the stress in B5_H300 is highly inhomogeneous in the streamwise direction even above the hills. Nevertheless, we can still calculate horizontally averaged properties as before, and compare them to those obtained in homogeneous runs.

Figure 8a shows the τ_{av} profiles from the simulations with $h_3\text{\_surf} = -0.0005$ m^2 s^{-3} and varying hill height. In spite of the highly inhomogeneous nature of the fields being averaged to make these profiles, they continue to vary smoothly and have qualitatively similar shapes. Furthermore, extrapolation of the profiles down to $z = 0$ m again gives a value consistent with the simulated total force on the surface in each case. As in the neutral cases, increasing surface force is also associated with increasing boundary layer depth although, with the shallow undisturbed stable boundary layer, the fractional changes in depth are much larger in stable conditions. This is discussed in more detail below. The U_{av} profiles (Fig. 8b) show slightly decreasing wind speeds and shear within the boundary layer as h increases. The pronounced regions of supergeostrophic speeds, visible toward the top of the boundary layer in the flat and low hills runs, also tend to disappear.

As noted above, the presence of the hills leads to a significant deepening of the stable boundary layer as h increases. For example, moving from flat B5_H0 to hilly B5_H300 almost doubles z_i from 360 to 710 m, while B3_H0 and B3_H300 have values of 550 and 960 m, respectively. The increases in depth over the hills are much larger than the hill amplitudes (150 m), indicating that they are not simply due to a displacement effect, which could be removed by changing the assumed displacement height.

A well-established formula for the depth of the stable boundary layer is that of Zilitinkevich (1972), which predicts that z_i should be proportional to $(u_* L/|f|)^{1/2}$. Although more complex formulas have recently been proposed that take into account a wider variety of length scales (e.g., Zilitinkevich and Mironov 1996), the original is reasonably successful in predicting the boundary layer depth for all but the least stable of the flat runs, with $z_i/(u_* L/|f|)^{1/2}$ having an approximately constant value (e.g., from Table 1, it is equal to 0.39 for B3_H0 and 0.40 for B5_H0). If the area-averaged stable boundary layer over hills really does act in the same way as a homogeneous boundary layer with the same values of surface momentum and buoyancy flux, then we would expect the same expression to hold with u_* and L replaced by their effective values [u_*^{eff} and $L^{\text{eff}} = -(u_*^{\text{eff}})^3/(\kappa h_3\text{\_surf})$, where κ is the von Kármán constant]. However, Fig. 9 shows that, although, as discussed previously, the values of z_i increase with increasing hill height, the rate of increase is not as fast as that of $(u_*^{\text{eff}} L^{\text{eff}}/|f|)^{1/2}$. In fact, we obtain $z_i/(u_*^{\text{eff}} L^{\text{eff}}/|f|)^{1/2} = 0.29$ for B3_H300 and 0.34 for B5_H300. One-dimensional runs with enhanced roughness length (dotted lines in Fig. 9) do show z_i varying approximately linearly with $(u_*^{\text{eff}} L^{\text{eff}}/|f|)^{1/2}$. This confirms that the area-averaged boundary layers over the hills truly are acting rather differently to homogeneous ones, as it excludes the possibility that the changes in normalized depth with increasing h are simply due to the extra momentum flux making the boundary layers insufficiently stable for the Zilitinkevich (1972) relation to be applicable. Furthermore, the example shown in Fig. 8 shows that, while a one-dimensional run with $h_3\text{\_surf} = -0.0005$ m^2 s^{-3} and $z_0^{\text{eff}} = 5$ m provides the same total surface force as B5_H300, it does not give a very good match to the U_{av} profile. In particular, it continues to show a supergeostrophic region close to the boundary layer top, which, as noted earlier, is not seen in the hilly run.

Some attempts have been made to see whether it is possible to improve the performance of the one-dimensional model by, in addition to changing the surface properties (i.e., the roughness length), also making changes to the parameterization of mixing in the boundary layer interior. The motivation for this is that a diagnosis of the area-averaged nondimensional shear [$\phi_m^{\text{eff}} = (\kappa z/u_*^{\text{eff}})S$] from the hilly runs (not shown) does indicate a stronger dependence on stability with increasing h. For example, while B5_H0 gave $\phi_m \simeq 1 + 3z/L$ in the lower boundary layer, the results for B5_H300 were more closely matched by $\phi_m^{\text{eff}} = 1 + 6z/L^{\text{eff}}$. The increased stability dependence can be mimicked in the one-dimensional model by decreasing the critical Rich-

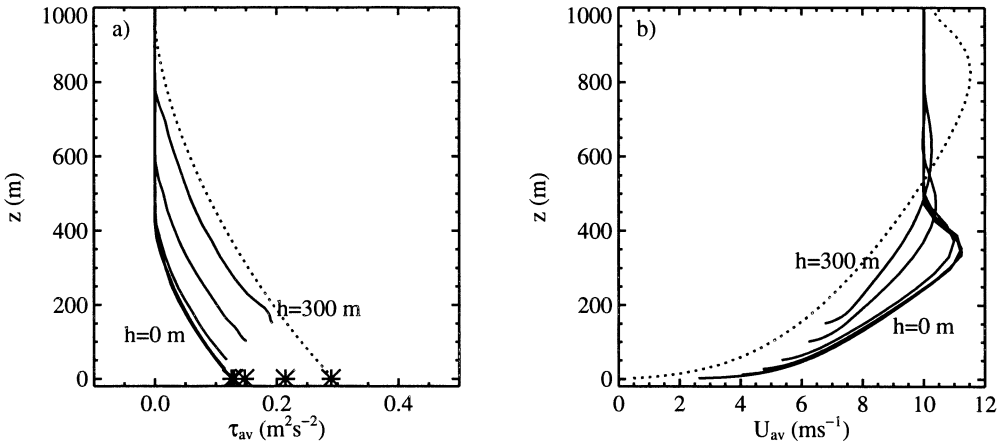

FIG. 8. Results from the stable simulations with h_3-surf $= -0.0005$ m^2 s^{-3} and $h = 0$, 20, 50, 100, 200, and 300 m (solid lines, although note that the 0-, 20-, and 50-m results are almost indistinguishable from one another). Also shown are the results from a one-dimensional simulation with the same value of surface buoyancy flux and $z_0^{\text{eff}} = 5$ m (dotted lines). (a) The magnitude of the horizontally averaged stress. The asterisks show the total force on the surface (due to shear stress and pressure force) from the hilly simulations. (b) The magnitude of the horizontally averaged wind vector.

ardson number. Runs with this decreased to around 0.2 did show shallower boundary layers for the same surface stress (which was achieved by increasing the effective roughness length). However, the velocity profiles still did not closely match those from the hilly runs, and improved matches to the stress profiles from the hilly runs were only achieved through empirical tuning (i.e., without a model to predict the optimum stability functions and effective roughness length values). For these reasons this approach has not been pursued further.

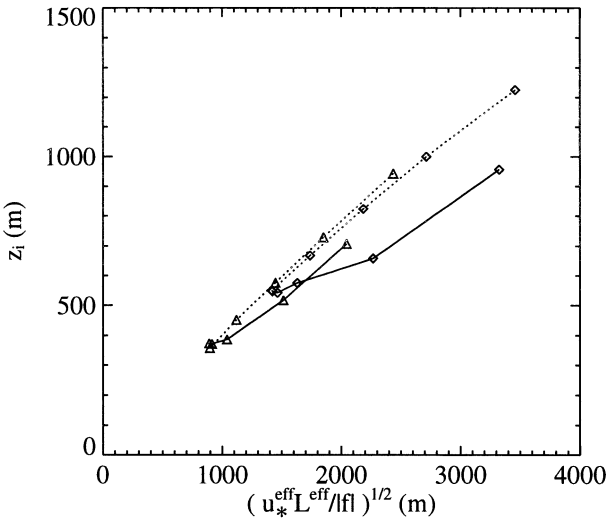

FIG. 9. Boundary layer depth diagnosed from stable runs as a function of $(u_*^{\text{eff}} L^{\text{eff}}/|f|)^{1/2}$. Solid lines show results from hilly simulations with varying hill height; dotted line shows results from one-dimensional simulations with varying effective roughness length. Diamonds represent h_3-surf $= -0.0003$ m^2 s^{-3}; triangles are h_3-surf $= -0.0005$ m^2 s^{-3}.

d. Evaluation of simplest parameterization

The preceding section has illustrated some limitations of the effective roughness length parameterization in stable conditions. However, it should be noted that the fractional errors in boundary layer depth in the cases examined were never greater than 30% and in most cases were considerably smaller. Furthermore, in terms of the synoptic development, the crucial quantity to predict accurately is the total force on the surface. Hence, in this section we assess how accurately the simplest parameterization using an effective roughness length that is itself independent of stability can reproduce the values of $(u_*^{\text{eff}})^2$ from our simulations. This is of practical interest as effective roughness length parameterizations are already in use in a number of large-scale models. Also, while the Met Office implementation (Milton and Wilson 1996) does apply an arbitrarily chosen correction to the roughness length in stable conditions, in practice, its impact is small and z_0^{eff} remains close to its neutral value in most cases with significant stress.

The solid lines in Fig. 10 show $(u_*^{\text{eff}}/G)^2$ as a function of h_3-surf$/(G^2|f|)$ from the two-dimensional hilly runs with various values of h. The increases in $(u_*^{\text{eff}}/G)^2$ occurring (for each h) between h_3-surf$/(G^2|f|) = 0.0$ and -0.01 are purely an artifact of the neutral simulations having been run for longer than the others, and should therefore be disregarded. The decreases in $(u_*^{\text{eff}}/G)^2$ with further increases in surface cooling then reflect the changes in the surface turbulent stresses and pressure force that were shown in Fig. 5. For small values of h they are primarily due to the surface turbulent stress decreasing with increasing stability, while for $h = 300$ m, the stronger variation of $(u_*^{\text{eff}}/G)^2$ with stability is predominantly due to the changes in the pressure force.

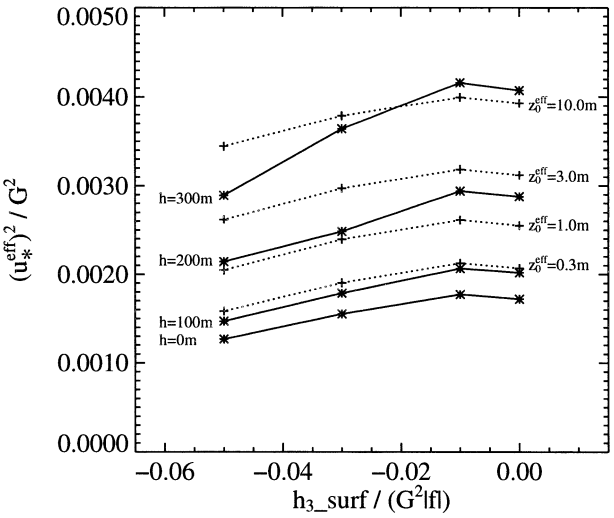

FIG. 10. Normalized total surface drag $(u_*^{eff}/G)^2$ as a function of normalized imposed surface buoyancy flux h_3_surf/$(G^2|f|)$. The solid lines show the results from the two-dimensional simulations with varying hill height. The dotted lines show the results from one-dimensional simulations with varying values of effective roughness length.

The dotted lines in Fig. 10 show the results obtained with a one-dimensional model (with different values of z_0^{eff}) as a function of h_3_surf/$(G^2|f|)$. If the dotted lines were exactly parallel to the solid lines, then this would indicate that a parameterization with z_0^{eff} independent of stability is optimum. In fact, for small values of h the lines are reasonably close to parallel. For larger values of h the differences are rather more marked, with a z_0^{eff} chosen to give the correct drag surface force in neutral conditions leading to some overprediction of the force in stable conditions. Nevertheless continuing to use the neutral value of z_0^{eff} would only mean using a value ($\simeq$10 m) that was a factor of 2 greater than the optimum value ($\simeq$5 m) for case B5_H300, and this may not be particularly significant compared to other uncertainties (such as our ability to accurately specify the appropriate neutral values). Furthermore, it is likely to be difficult to develop a robust parameterization of the relatively weak dependence of z_0^{eff} on stability, as the results suggest that it is likely to be highly sensitive to the detailed hill geometry (e.g., with cases less prone to pooling of cold air in valleys showing a weaker dependence on stability). These arguments suggest that current knowledge does not, for the purposes of momentum transfer, justify moving beyond the simplest approach of using z_0^{eff} independent of stability.

4. Conclusions

This paper has presented results from numerical simulations examining the impact of moderate orography on the stable boundary layer. Various flow features (e.g., fractional speed-up; tendency to decoupled flow in valleys in more stable conditions) have been shown to be qualitatively consistent with observations. However, the major focus has been on the diagnosis of area-averaged quantities (such as surface forces and boundary layer depth) which, while key for parameterization schemes, are very difficult to obtain directly from observations.

In all of the cases studied, the changes in the total surface force with changing hill height have been found to be dominated by the changes in the pressure force, with the changes in the surface turbulent stresses being smaller. This is consistent with the neutral results of Wood and Mason (1993). For low hills all but the most stable runs show the expected increase with stability in nondimensional pressure force due to the enhanced shear (Belcher and Wood 1996). With the surface stress decreasing with increasing stability, the absolute values of the force are almost independent of stability. With larger hills a stronger dependence on stability is apparent, although even in the most stable case with the largest hill, the pressure force is over 50% of its neutral value. Furthermore, even this reduction may be excessive, as it appears to be associated with pooling of cold air in the valleys—a process that is likely to be exaggerated in these two-dimensional simulations. Future runs with three-dimensional topography will be required to investigate this further.

With the modeled hills in some cases having peak-to-trough heights comparable to the undisturbed boundary layer depth, the resulting boundary layers are often highly inhomogeneous. However, examination of the area-averaged fluxes makes it clear that the average depth of mixing is increased. Our diagnosed boundary layer depths have been compared with those predicted using the Zilitinkevich (1972) parameterization, with the surface fluxes replaced by their effective values (i.e., including the pressure force in the surface stress). The agreement is reasonable, although the parameterization overestimates the rate of deepening with increasing hill height.

The boundary layer depth results (and other more detailed diagnostics) suggest that, perhaps unsurprisingly, it is rather oversimplistic to attempt to interpret the area-averaged stable boundary layer over hills as being equivalent to a homogeneous boundary layer with the same values of surface momentum and buoyancy flux. In principle a distributed drag parameterization scheme such as that recently proposed by Wood et al. (2001) might offer enough flexibility to make it possible to capture these differences. However, considerable further work on the design and evaluation of the scheme will be required. In the meantime, an issue of key practical significance is whether use of the simpler effective roughness length parameterizations, already widely used in the large-scale models, leads to significant errors. Encouragingly in this respect, one-dimensional model runs with an effective roughness length independent of stability have been shown to be reasonably successful

in reproducing the total surface forces from the hilly simulations.

Acknowledgments. The authors wish to acknowledge the contributions to this work of Steve Derbyshire, Alan Grant, and Fiona Hewer.

REFERENCES

Belcher, S. E., and N. Wood, 1996: Form and wave drag due to stably stratified turbulent flow over low ridges. *Quart. J. Roy. Meteor. Soc.,* **122,** 863–902.

Calhoun, R. J., R. L. Street, and J. R. Koseff, 2001: Turbulent flow over a wavy surface: Stratified case. *J. Geophys. Res.,* **106,** 9295–9310.

Clark, T. L., 1977: A small-scale dynamic model using a terrain-following transformation. *J. Comput. Phys.,* **24,** 186–215.

Coppin, P. A., E. F. Bradley, and J. J. Finnigan, 1994: Measurements of flow over an elongated ridge and its thermal stability dependence: The mean field. *Bound.-Layer Meteor.,* **69,** 173–199.

Derbyshire, S. H., 1990: Nieuwstadt's stable boundary layers revisited. *Quart. J. Roy. Meteor. Soc.,* **116,** 127–158.

——, 1995: Stable boundary layers: Observations, models and variability. Part I: Modelling and measurements. *Bound.-Layer Meteor.,* **74,** 19–54.

——, and N. Wood, 1994: The sensitivity of stable boundary layers to small slopes and other influences. *Proc. Fourth IMA Conf. on Waves and Stably-Stratified Turbulence,* Oxford, United Kingdom, Institute of Mathematics and Its Applications, 105–118.

Frank, H., K. Heldt, S. Emeis, and F. Fiedler, 1993: Flow over an embankment: Speed-up and pressure perturbation. *Bound.-Layer Meteor.,* **63,** 163–182.

Grant, A. L. M., 1994: Wind profiles in the stable boundary layer, and the effect of low relief. *Quart. J. Roy. Meteor. Soc.,* **120,** 27–46.

——, and P. J. Mason, 1990: Observations of boundary-layer structure over complex terrain. *Quart. J. Roy. Meteor. Soc.,* **116,** 159–186.

Henn, D. S., and R. I. Sykes, 1999: Large-eddy simulation of separated flow over hills. *J. Fluid Mech.,* **383,** 75–112.

Hignett, P., and W. P. Hopwood, 1994: Estimates of effective surface roughness over complex terrain. *Bound.-Layer Meteor.,* **68,** 51–73.

Holden, J. J., S. H. Derbyshire, and S. E. Belcher, 2000: Tethered balloon observations of the nocturnal stable boundary layer in a valley. *Bound.-Layer Meteor.,* **97,** 1–24.

Hunt, J. C. R., K. J. Richards, and P. W. M. Brighton, 1988: Stratified airflow over one or two hills. *Quart. J. Roy. Meteor. Soc.,* **114,** 859–866.

Inglis, D. W. F., T. W. Choularton, I. M. F. Stromberg, B. A. Gardiner, and M. Hill, 1995: Testing of a linear airflow model for flow over complex terrain subject to stable, structured stratification. *Wind and Trees,* M. P. Coutts and J. Grace, Eds., Cambridge University Press, 88–132.

Leonard, B. P., M. K. MacVean, and A. P. Lock, 1993: Positivity-preserving numerical schemes for multidimensional advection. NASA Tech. Memo. 106055, ICOMP-93-05, 62 pp.

Mason, P. J., 1987: Diurnal variations in flow over a succession of ridges and valleys. *Quart. J. Roy. Meteor. Soc.,* **113,** 1117–1140.

Milton, S. F., and C. A. Wilson, 1996: The impact of parameterized subgrid-scale orographic forcing on systematic errors in a global NWP model. *Mon. Wea. Rev.,* **124,** 2023–2045.

Piacsek, S. A., and G. P. Williams, 1970: Conservation properties of convection difference schemes. *J. Comput. Phys.,* **6,** 392–405.

Vosper, S. B., S. D. Mobbs, and B. A. Gardiner, 2002: Measurements of the near-surface flow over a hill. *Quart. J. Roy. Meteor. Soc.,* **128,** 2257–2280.

Weng, W., L. Chang, P. A. Taylor, and D. Xu, 1997: Modelling stably stratified boundary layer flow over low hills. *Quart. J. Roy. Meteor. Soc.,* **123,** 1841–1866.

Wood, N., 1995: The onset of separation in neutral, turbulent flow over hills. *Bound.-Layer Meteor.,* **76,** 137–164.

——, 1998: Turbulent fluxes in complex terrain and the effects of static stability. *Proc. ECMWF Orography Workshop,* Reading, United Kingdom, European Centre for Medium-Range Weather Forecasts, 23–50.

——, and P. J. Mason, 1993: The pressure force induced by neutral, turbulent flow over hills. *Quart. J. Roy. Meteor. Soc.,* **119,** 1233–1267.

——, A. R. Brown, and F. E. Hewer, 2001: Parameterizing the effects of orography on the boundary layer: An alternative to effective roughness lengths. *Quart. J. Roy. Meteor. Soc.,* **127,** 759–777.

Zilitinkevich, S. S., 1972: On the determination of the height of the Ekman boundary layer. *Bound.-Layer Meteor.,* **3,** 141–145.

——, and D. V. Mironov, 1996: A multi-limit formulation for the equilibrium depth of a stably stratified boundary layer. *Bound.-Layer Meteor.,* **81,** 325–351.